ELSEVIER

Polymer 43 (2002) 6341–6349

polymer

www.elsevier.com/locate/polymer

Structure and thermodynamic properties from molecular dynamics simulations of the polyethylene crystal

Emmanuel Duffour[a,*], Patrice Malfreyt[b]

[a]*Laboratoire Arc Electrique et Plasmas Thermiques, UMR CNRS 6069, 24 avenue des Landais, Université Blaise Pascal, 63177 Aubière Cedex, France*
[b]*Laboratoire de Thermodynamique des Solutions et des Polymères, UMR CNRS 6003, 24 avenue des Landais, Université Blaise Pascal, 63177 Aubière Cedex, France*

Received 2 March 2002; received in revised form 7 June 2002; accepted 9 June 2002

Abstract

This paper describes the results of molecular dynamics simulations of polyethylene crystal at two temperatures in the absence of periodic boundary conditions. We report the profiles of the temperature and pressure tensor along two directions in the crystal. We check that the two different methods (IK) and (MOP) for calculating the pressure tensor give similar profiles, which are constant in the middle of the crystal. In addition, we compare the data resulted from the pressure profiles with the values obtained from the virial route. The internal structure of the polyethylene is visualized through the intramolecular and intermolecular radial distribution functions. © 2002 Elsevier Science Ltd. All rights reserved.

Keywords: MD; Polyethylene crystal; Pressure tensor

1. Introduction

A knowledge of the thermodynamic properties of crystalline structures, solid state, in molecular system becomes possible using molecular dynamics simulations. This technique provides us with an atomic description, the dynamical behaviour and thermodynamic properties of the system. There have been a significant number of computational studies of crystal structures using both Monte Carlo and MD techniques [1–6].

Modelling and simulation of energetic particle–solid interactions have also been in progress during this last decade. The interactions of fullerene molecules with silicon surfaces [7], the ion bombardment of polyethylene [8], the hydrogen atom interactions with C_{60} [9] have been successfully studied using standard molecular dynamics simulations.

We plan also to study the bombardment of polyethylene crystal by some particles which give rise to important industrial applications. These calculations will be made in the scope of plasma physic application. Indeed, in this research field, there are several new industrial applications, especially in the plasma–plastic interaction field, like circuit breaker (PTFE/SF_6 interaction) or in the electrothermal gun for example [10–12]. So, in a short term, this polyethylene model will be used to consider the interaction between plasma and an insulating wall where an incident particle flow will interact with the latter. The particle flow will induce a pressure variation inside the polymer which will be evaluated with the two techniques used in this work.

Before doing so, we wish to explore our MD algorithm and compute some thermodynamic properties of this crystal. Our force field differs from those of the previous studies [8,13,14] and is composed of energetic contributions currently used in the molecular simulations. In this paper, we check the thermal and mechanical properties by computing the temperature and pressure tensors along some directions in the crystal without periodic boundary conditions. So far we know, the calculations of the temperature and pressure profiles have not yet been carried out on a solid structure as the polyethylene crystal.

In Section 2, we describe the derivation of the polyethylene crystal force field and the computational techniques we have employed in our simulations. In Section 3, we calculate the temperature and pressure profiles across the polyethylene. Finally, in Section 4 we draw the main conclusions from our work.

* Corresponding author.

PII: S0032-3861(02)00412-3

2. Computational method

2.1. United atom model

In the united atom (UA) model, the atom is represented by a spherical pseudo-atom with interaction site placed in the position of the carbon nucleus. In this model, each CH_3 and CH_2 groups are modelled by single Lennard-Jones interaction sites. Different potentials using UA model have already provided useful and experimentally relevant predictions of many aspects of polyethylene [15]. All united atoms on different chains or separated by more than three chemical bonds interact through a Lennard-Jones potential

$$V_{LJ}(r_{ij}) = 4\epsilon_{ij}\left[\left(\frac{\sigma_{ij}}{r_{ij}}\right)^{12} - \left(\frac{\sigma_{ij}}{r_{ij}}\right)^{6}\right] \quad (1)$$

where ϵ_{ij} is the energy parameter of the interaction, σ_{ij} is the Lennard-Jones core diameter and r_{ij} is the distance between interactions sites i and j. The LJ parameters for the interactions between CH_3 and CH_2 united atoms are calculated by using the Lorentz–Berthelot mixing rules and are reported in Table 1:

$$\epsilon_{CH_3-CH_2} = (\epsilon_{CH_3}\epsilon_{CH_2})^{1/2}\sigma_{CH_3-CH_2} = \frac{1}{2}(\sigma_{CH_3} + \sigma_{CH_2}) \quad (2)$$

The bond potential between two bonded united atoms i and j is described by a Morse oscillator [16,17]. This potential is given by Eq. (3), where r_{ij} is the internuclear separation between unit i and j, R_e is the equilibrium distance between the two units, D and α are constants given in Table 1

$$V_2(r_{ij}) = D[1 - \exp(-\alpha(r_{ij} - R_e))]^2 \quad (3)$$

The bond angle potential describing the interaction between three consecutive bonded atom units is given by Eq. (4), where θ_{ijk} is the bending angle, and θ_0 is the equilibrium angle. The constants K and θ_0 are given in Table 1

$$V_3(\theta_{ijk}) = \mathrm{SW}(r_{ij})\mathrm{SW}(r_{jk})\frac{K}{2}(\cos\theta_{ijk} - \cos\theta_0)^2 \quad (4)$$

where $\mathrm{SW}(r_{ij})$ and $\mathrm{SW}(r_{jk})$ are the switching functions between united atoms (i,j) and (j,k), respectively.

The torsional potential function describes the interactions arising from torsional forces in chain between four consecutive united atoms. ϕ_{ijkl} is the dihedral angle, A, B and C are constants given in Table 1. This potential results in a *gauche–trans* energy difference of 2.5 kJ mol^{-1} and a *cis*-barrier of 16.7 kJ mol^{-1} [15]

$$V_4(\phi_{ijkl}) = \mathrm{SW}(r_{ij})\mathrm{SW}(r_{jk})\mathrm{SW}(r_{kl})\mathrm{SW}(\theta_{ijk})\mathrm{SW}(\theta_{jkl})(A - B\cos\phi_{ijkl} + C\cos^3\phi_{ijkl}) \quad (5)$$

where $\mathrm{SW}(\theta_{ijk})$ and $\mathrm{SW}(\theta_{jkl})$ are the switching bending functions between three consecutive atoms (i,j,k) and (j,k,l), respectively.

Switching functions $\mathrm{SW}(r)$ and $\mathrm{SW}(\theta)$ depending on the distance and the valence angle, respectively, are used in the bond angle and torsional potentials to attenuate them to zero when the corresponding bonds are extended and are ultimately broken. Concerning $\mathrm{SW}(r)$, different forms exist, but we use the trigonometric function given by Eq. (6)

$$\mathrm{SW}(r) = 1.0 - \tanh[1.53131681\times10^{-7}(r - R_e)(r + 4.669625)^8] \quad (6)$$

In the $V_4(\phi_{ijkl})$ potential, a term as $(\sin\theta)^{-1}$ is taking into account in its derivative. So, when the angle θ is close to π, the potential becomes singular, and the corresponding force is infinite. Thus, a bending switching function must be added to the potential $V_4(\phi_{ijkl})$ to make up for this singularity. This function is given by Eq. (7)

$$\mathrm{SW}(\theta) = (1 - \cos^{16}\theta)^4 \quad (7)$$

2.2. Simulation details

Our model consists of N_c polyethylene chains ($N_c = 72$) containing N_a CH_2 groups ($N_a = 100$) oriented along z-axis. The thickness of this initial configuration is approximately 12.6 nm. In the orthorhombic phase, two chains of polyethylene make up the unit cell in which the parameters a (0.74 nm), b (0.49 nm) and c (0.26 nm) are parallel to x, y and z axes, respectively. Our system contains $N_t = 7200$ atoms. A polyethylene crystal picture is shown in Fig. 1. The dimensions of the crystal are $L_x = 4.8$ nm, $L_y = 2.8$ nm and $L_z = 12.6$ nm.

In addition, the two end units of the one hundred units polyethylene chain are bonded to hypothetical infinite mass fixed units. This arrangement is commonly referred as *nanospring* [18]. We have chosen to restrain only the z-direction to be able to study the destruction of the crystal under particle collisions in a next work. The inclusion of switching functions in the energetic potential functions has been achieved with this aim.

2.3. Integration method

Most of the simulations of crystals use symplectic integrators which are in fact particular algorithms for generating approximate solutions of the Hamiltonian system of ordinary differential equations. The equations of motion, Hamilton's equation, are given by

$$\frac{\partial p_i}{\partial t} = \dot{p}_i = -\frac{\partial H}{\partial q_i}, \qquad \frac{\partial q_i}{\partial t} = \dot{q}_i = \frac{\partial H}{\partial p_i} \quad (8)$$

where (q_i, p_i), $i = 1,\ldots,N_t$ is a set of N_t canonically conjugated coordinates and momenta, and H is the classical Hamiltonian function.

Unlike many numerical methods for solving sets of ordinary differential equations, symplectic integrators are specifically tailored to Hamiltonian systems because they

Table 1
Force field parameters. Bonds, angle, torsional and van der Waals parameters

Potential	Parameters	
$V_2(r_{ij})$	$D = 334.720$ kJ/mol	
	$R_e = 0.153$ nm	
	$\alpha = 19.9$ nm^{-1}	
$V_3(\theta_{ijk})$	$K = 130.220$ kJ/mol	
	$\theta_0 = 1.9540837$ rad	
$V_4(\phi_{ijkl})$	$A = 8.370$ kJ/mol	
	$B = 18.410$ kJ/mol	
	$C = 26.780$ kJ/mol	
$V_{LJ}(r_{ij})$	$\sigma_{CH_2} = 0.3980$ nm	$\sigma_{CH_3} = 0.3980$ nm
	$\epsilon_{CH_2} = 477$ J/mol	$\epsilon_{CH_3} = 477$ J/mol

satisfy the symplectic property that exact solutions to Eq. (8) must satisfy. This implies that approximate solutions generated by the symplectic integrator preserve the N_t Poincare integral invariants of the Hamiltonian system [19].

The Hamiltonian of the system is made up of a kinetic contribution depending solely on the conjugated momenta and of a potential contribution depending only on the generalized coordinates. The integration of the Hamiltonian system requires an explicit Runge–Kutta–Nyström method using a symplectic integrator developed by Calvo and Sanz-Serna (five stage, fourth order) [18]. The set of the integrator coefficients is given in Table 2.

The equation of motion are integrated using a time-step of 2 fs. The simulation time is about 15 ps. The crystal needs approximately 3 ps to reach its equilibrium state and the acquisition time is 10 ps. The production phase where thermodynamical and structural quantities are collected consists of 500 configurations, each configuration being saved at every 20 fs. Intermolecular and intramolecular interactions have been computed using a large cutoff $r_c = 2$ nm. The simulation has been performed in the

Table 2
Integrator coefficients of the symplectic integrator

$a[k]$	$b[k]$
$a[1] = 0.205177661542290$	$b[1] = 0.061758858135626$
$a[2] = 0.403021281604210$	$b[2] = 0.338978026553640$
$a[3] = -0.120920876338910$	$b[3] = 0.614791307175580$
$a[4] = 0.512721933192410$	$b[4] = -0.140548014659370$
$a[5] = 0.000000000000000$	$b[5] = 0.125019822794530$

microcanonical NVE ensemble without applying any periodic boundary conditions.

Initial condition settings consist in placing all units in the crystal, in their equilibrium position; the distance between two adjacent units is equal to R_e, and θ and ϕ angle values are set to minimize the potentials V_3 and V_4, respectively. For conjugated momenta, random velocities between $\pm V_{max}$, are computed according to the following relationships

$$\sum_{i=1}^{N_t} p_i = 0, \qquad \sum_{i=1}^{N_t} \frac{p_i^2}{2M_{CH_2}} = \frac{3}{2} N_t k_B T \tag{9}$$

where N_t is the total number of units in the crystal, k_B is Boltzmann's constant, and T is the temperature. In fact, initial velocities have been selected randomly from a Gaussian distribution by checking also that the sum over all the momenta has been equal to zero. The simulations have been run on Pentium Pro workstations and typically required three weeks of CPU time.

3. Results and discussions

Fig. 2 presents the total energy of the system as a function of time for two temperatures. The mean energy values are also given in Table 3. This figure demonstrates that the total energy of the system is well conserved with deviations less than 0.1%. This result validates the time step size and underlines the efficiency and the stability of the

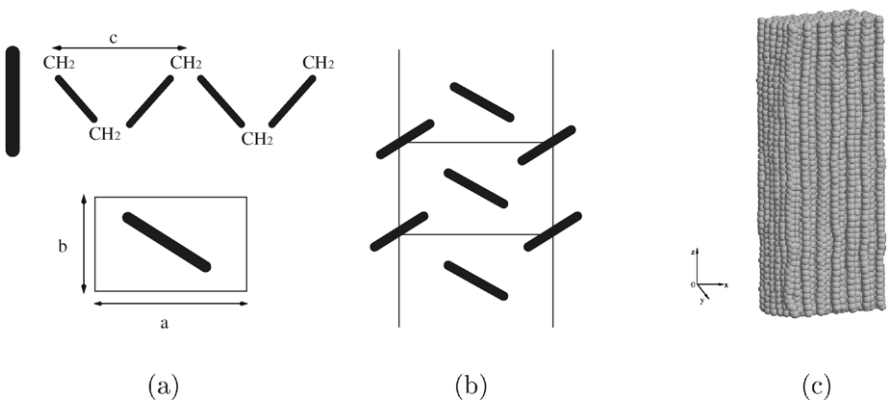

Fig. 1. A schematic representation of (a) the unit cell, (b) the orthorhombic phase. A schematic diagram of the configuration of the polyethylene crystal is displayed in (c) with 7200 united atoms.

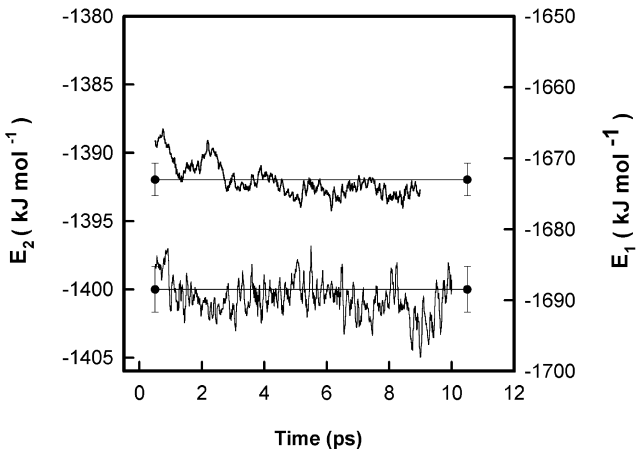

Fig. 2. Instantaneous total energy E_1 ($T = 217$ K) and E_2 ($T = 312$ K) of the crystal as of function of time at two temperatures.

sympletic integrator used in our simulations from the energy point of view. The trajectories of the temperature of the system are shown in Fig. 3. These plots highlight that the temperature stays constant throughout the simulation runs within a deviation of about 1% (Table 3).

Table 3
Average temperature T (K), the calculated pressure tensor components resulted from the virial route (MPa), and the trace of the pressure tensor (MPa)

	Set 1	Set 2
T	217_2	312_2
p_{xx}	17.5	31.7
p_{xy}	0.08	−0.63
p_{xz}	−0.28	−0.06
p_{yy}	−7.62	−8.00
p_{yx}	0.10	−0.59
p_{yz}	−0.80	0.13
p_{zz}	1.17	1.67
p_{zx}	0.02	0.03
p_{zy}	−0.01	0.05
$p = (1/3)(p_{xx} + p_{yy} + p_{zz})$	2.51	6.82
$E_{\text{stretching}}$	107.6_{15}	148.6_{18}
E_{bending}	64.6_{11}	95.4_{19}
E_{torsion}	-767.4_{12}	-731.8_{14}
$E_{\text{non-bonded}}$	-1349_2	-1302_3
E_{total}	-1674_2	-1400_2

The average bond, bond angle, torsional and non-bonded energetic contributions (kJ mol^{-1}) are reported. The total energy includes the kinetic energy part. The subscript indicates the accuracy of the last decimal(s). The number 217_2 means 217 ± 2 and $107.6_{15} = 107.6 \pm 15$.

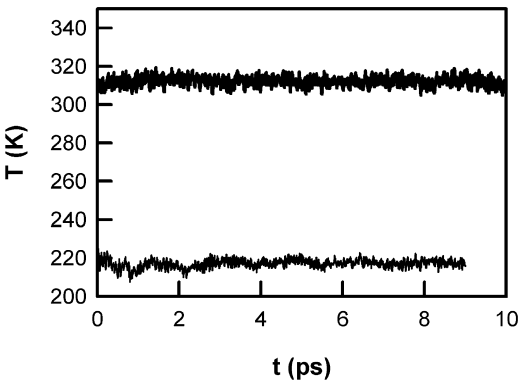

Fig. 3. Trajectories of the temperature of the crystal as a function of time for the two studied temperatures.

The components of the molecular temperature tensor are calculated using the following expression

$$T_{\alpha\beta}(z) = \frac{\sum_i^{N_c} H(z_i)(v_i)_\alpha \cdot (v_i)_\beta}{\sum_i^{N_c} H(z_i)} \tag{10}$$

where $(v_i)_\alpha$ is the α component of the velocity of the centre of mass of chain i and $H(z_i)$ is a top-hat function

$$H(z_i) = \begin{cases} 1 & \text{for } z - \dfrac{\Delta z}{2} < z_i < z + \dfrac{\Delta z}{2} \\ 0 & \text{otherwise} \end{cases} \tag{11}$$

Fig. 4a shows the average temperature profile $T(z)$ along the z-direction. $T(z)$ is defined as the trace of the temperature tensor. We see that this component fluctuates about the average value of the total temperature within the deviation previously calculated. Actually, the mean value of $T(z)$ coincides exactly with the temperature computed from the kinetic energy Eq. (9). Fig. 4b presents one off-diagonal element of the pressure tensor $T_{xz}(z)$ as a function of the z-axis. This component oscillates around zero with an average value equal to −0.4 K and a standard deviation of 2.0 K. We checked also that the remaining off-diagonal element of the temperature tensor are close to zero across the box and that the on-diagonal elements of the temperature are identical within the statistical fluctuations both along a given direction and in the three Cartesian directions. This is indicative of the correct equipartition of the energy among the translational degrees of freedom of the chains.

The element $\alpha\beta$ of the molecular pressure tensor is defined in terms of the virial expression according to Eq. (12)

$$p_{\alpha\beta} = \frac{1}{V}\sum_{i=1}^{N_c} m_i (v_i)_\alpha (v_i)_\beta + \sum_{i=1}^{N_c-1}\sum_{j>i}^{N_c}\sum_{a=1}^{N_u}\sum_{b=1}^{N_u} (\mathbf{r}_{ij})_\alpha (\mathbf{f}_{iajb})_\beta \tag{12}$$

where V is the volume of the system, m_i and v_i are the

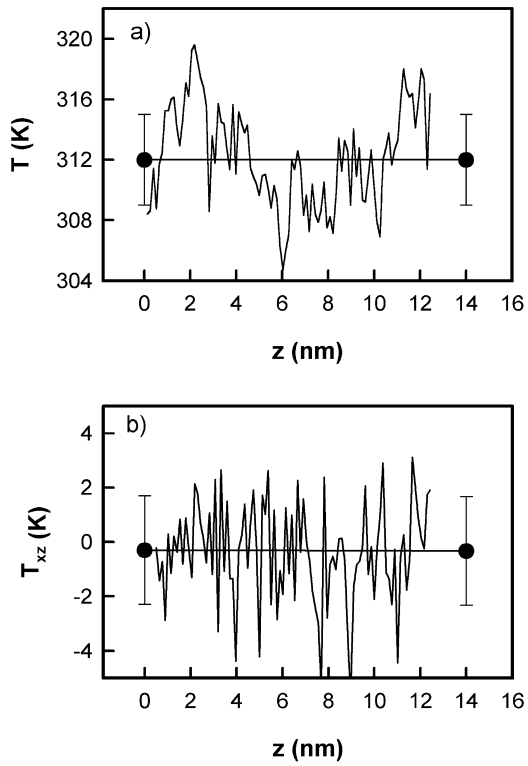

Fig. 4. Temperature profiles along the z-direction (a) $T(z)$ and (b) $T_{xz}(z)$ at $T = 312$ K. $T(z)$ is defined as the trace of the temperature tensor. The straight lines correspond to the average temperature along the z-axis with error bars representing rms fluctuations.

molecular mass and velocity of the centre of mass, respectively, $\mathbf{r}_{ij}$ is the vector between the centre of mass of chains i and j and

$$\mathbf{f}_{iajb} = -\frac{\mathbf{r}_{iajb}}{r_{iajb}} \frac{\mathrm{d}U(r_{iajb})}{\mathrm{d}r_{iajb}} \tag{13}$$

$\mathbf{f}_{iajb}$ is the force between atom a in chain i and atom b in chain j, r_{iajb} being the distance between atom a in chain i and atom b in chain j. In addition, we compute the components of the molecular pressure tensor as function of the x and y directions using two different methods.

Fig. 5 plots the pressure of the system and its average as a function of time. The pressure is calculated using Eq. (12) and the time average components of the pressure tensor are given in Table 3. As expected, the average pressure converges to a stable value although the instantaneous pressure fluctuates very much about the mean value within 11.6 MPa and with two extrema values of -20.5 and 30.6 MPa. Table 3 shows that the off-diagonal elements of the molecular pressure tensor are close to zero as expected for a system at mechanical equilibrium. We see that the on-diagonal elements are not all equal but we can estimate the hydrostatic pressure as $p = (p_{xx} + p_{yy} + p_{zz})/3$. The fact that the on-diagonal elements are not equal can be due to inappropriate parameters for the non-bonded potentials [5]. The absence of boundary periodic conditions can play a significant role with the geometry of the crystal. A more detailed analysis in the interior of the crystal along some particular directions can be performed using the following methods.

The Irving–Kirkwood [20,21] definition for a molecular system leads to the following expression:

$$p_{\alpha\beta}(y) = \frac{1}{V} \sum_{i,\alpha\beta} H(y_i) m_i (v_i)_\alpha (v_i)_\beta + \frac{1}{A} \left\langle \sum_{i=1}^{N_c-1} \sum_{j>i}^{N_c} \sum_{a=1}^{N_u} \sum_{b=1}^{N_u} (\mathbf{r}_{ij})_\alpha \times (\mathbf{f}_{iajb})_\beta \frac{1}{|y_{ij}|} \theta\left(\frac{y - y_i}{y_{ij}}\right) \theta\left(\frac{y_j - y}{y_{ij}}\right) \right\rangle \tag{14}$$

In this equation, $\langle \cdots \rangle$ denotes an ensemble time average. $\theta((y - y_i)/y_{ij})$ is the unit step function which is equal to 1 when $((y - y_i)/y_{ij}) > 0$ and zero otherwise. The distance y_{ij} is divided into slabs of width Δy and the chains i and j contribute to the pressure tensor in a particular slab if the line joining i and j, crosses, starts or finishes in the slab. The contribution from i–j interaction is distributed uniformly along the line joining the centre of mass of chains i and j.

In this study, we use also an additional statistical mechanical technique [22,23], commonly referred as the method of planes (MOP), for calculating the pressure tensor. An alternative definition of the molecular pressure tensor is given by

$$p_{\alpha y}(y) = \frac{1}{2A} \left\langle \sum_{i=1}^{N_c} m_i (v_i)_\alpha \frac{\mathrm{d}}{\mathrm{d}t} \mathrm{sgn}[y_i - y] \right\rangle + \frac{1}{A} \sum_{i=1}^{N_c-1} \sum_{j>i}^{N_c} \sum_{a=1}^{N_u} \sum_{b=1}^{N_u} (\mathbf{f}_{iajb})_\alpha [\theta(y_i - y)\theta(y - y_j) - \theta(y_j - y)\theta(y - y_i)] \tag{15}$$

if y_i and y_j are both either smaller or larger than y, the contribution to the pressure tensor is zero. If $y_i < y$ and $y_j > y$ then the first product of the Heaviside functions is zero while the second is unity. If $y_i > y$ and $y_j < y$ then the second is unity while the first is unity. The kinetic part of the pressure tensor is due to the momentum flux across the plane A. If a particle i crosses the plane during time interval between t and $t + \Delta t$, we use the sign of the y component of the velocity to check whether the crossing is from right to left or vice versa.

In a first time, we see that the pressures calculated from the IK and the MOP methods match very well (Fig. 6) validating both these methods for this type of study. We check also that the off-diagonal elements along both x and y directions oscillates around zero indicating that the system is at mechanical equilibrium. We observe that the p_{xx} presents a plateau in the middle of the crystal. The deviations from the plateau are located near the boundaries and are due the absence of periodic boundary conditions.

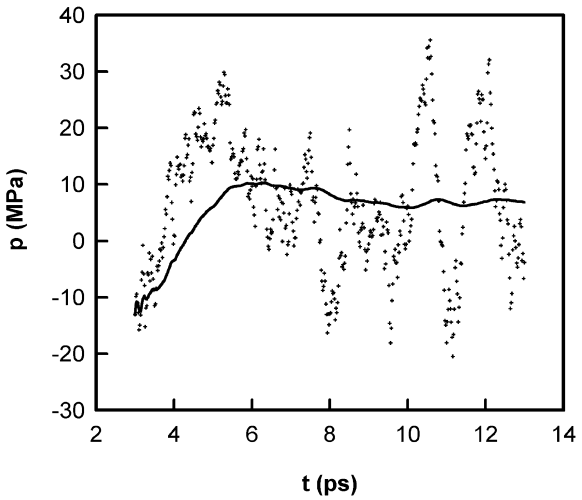

Fig. 5. Instantaneous pressure (···) and average pressure (—) calculated from the virial route Eq. (12) as a function of time for the polyethylene crystal.

The average p_{xx} pressure can be deduced from an average of the values within the plateau and give a better knowledge of the internal pressure than the values deduced from the virial route. An average value of p_{xx} along the x-direction is 21.5 ± 1.2 MPa at $T = 217$ K and 37.0 ± 4.6 MPa at $T = 312$ K. The weak standard deviations allow a good estimation of the component of internal pressure inside the crystal. It is interesting to note that the p_{yy} component along the y-axis presents a different profile with a smaller plateau located in the negative pressures in agreement with the values calculated from the virial formula within the statistical uncertainty inherent in the calculation of the pressure, ($p_{yy} = -3.8 \pm 0.3$ MPa at $T = 217$ K, $p_{yy} = -4.4 \pm 1.7$ MPa at $T = 312$ K). The absence of periodic boundary conditions is also well noticeable on the profile of this component close to the boundaries. We see that the plateau has shrunk in the y-direction. This may be explained by the smaller dimension of the crystal over this direction. In this case, the absence of periodic boundary conditions affects further the profiles of this pressure component. The negative component p_{yy} along the y-axis denotes a certain tension in the coil which is consistent with the comparison between the $y-z$ and $x-z$ projections of the crystal in the simulations (Fig. 7). As the temperature increases, we observe an increase in the p_{xx} component of the pressure tensor.

As concerns the stable structure resulted from our simulations, we check that it is in orthorhombic phase. The a, b and c parameters calculated from the centre of masses of every chain at $T = 217$ K over 10 ps are equal to 0.77 ± 0.01, 0.46 ± 0.01 and 0.25 ± 0.01 Å, respectively. The difference between the average and initial a and b

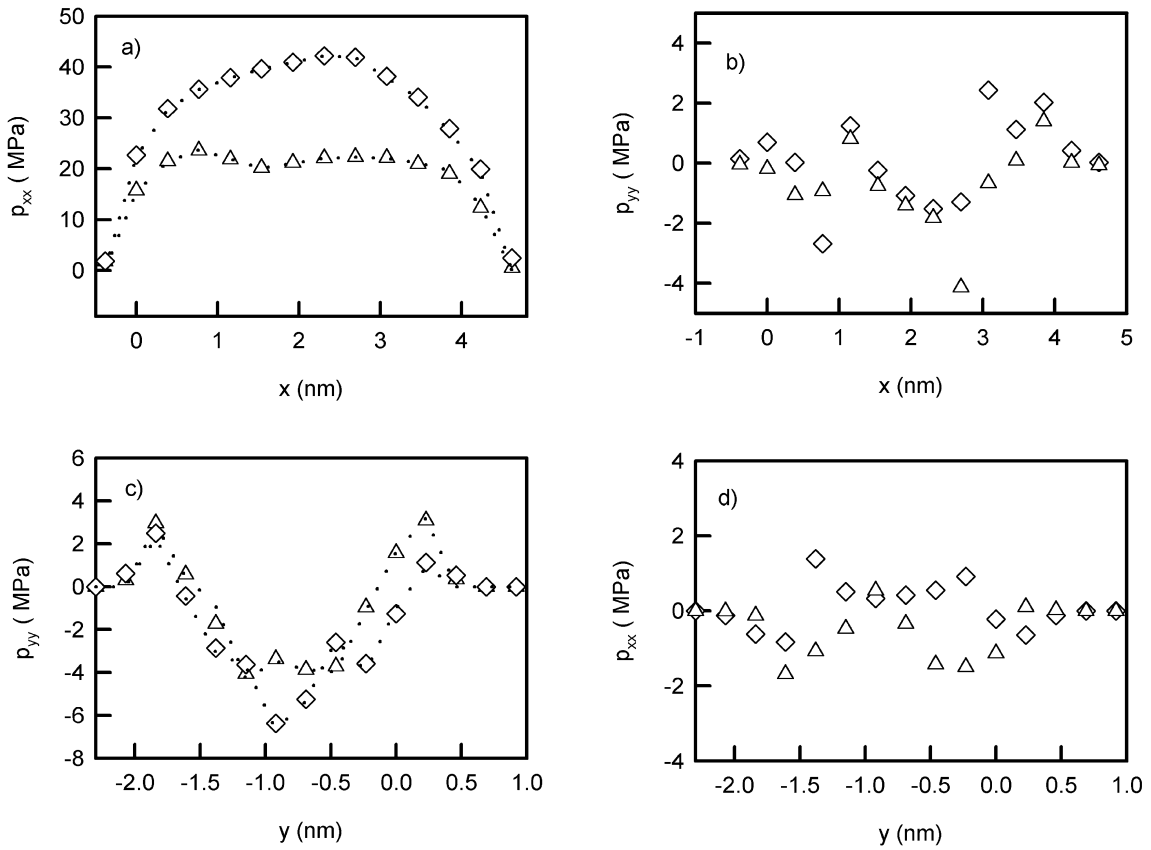

Fig. 6. Component pressure profiles calculated from the IK definition at $T = 217$ K (△) and $T = 312$ K (◇) and from the MOP definition (···) for the two temperatures. (a) $p_{xx}(x)$; (b) $p_{yy}(x)$; (c) $p_{yy}(y)$; (d) $p_{xx}(y)$. In (b) and (d) cases, the profiles calculated from the MOP definition are omitted for clarity.

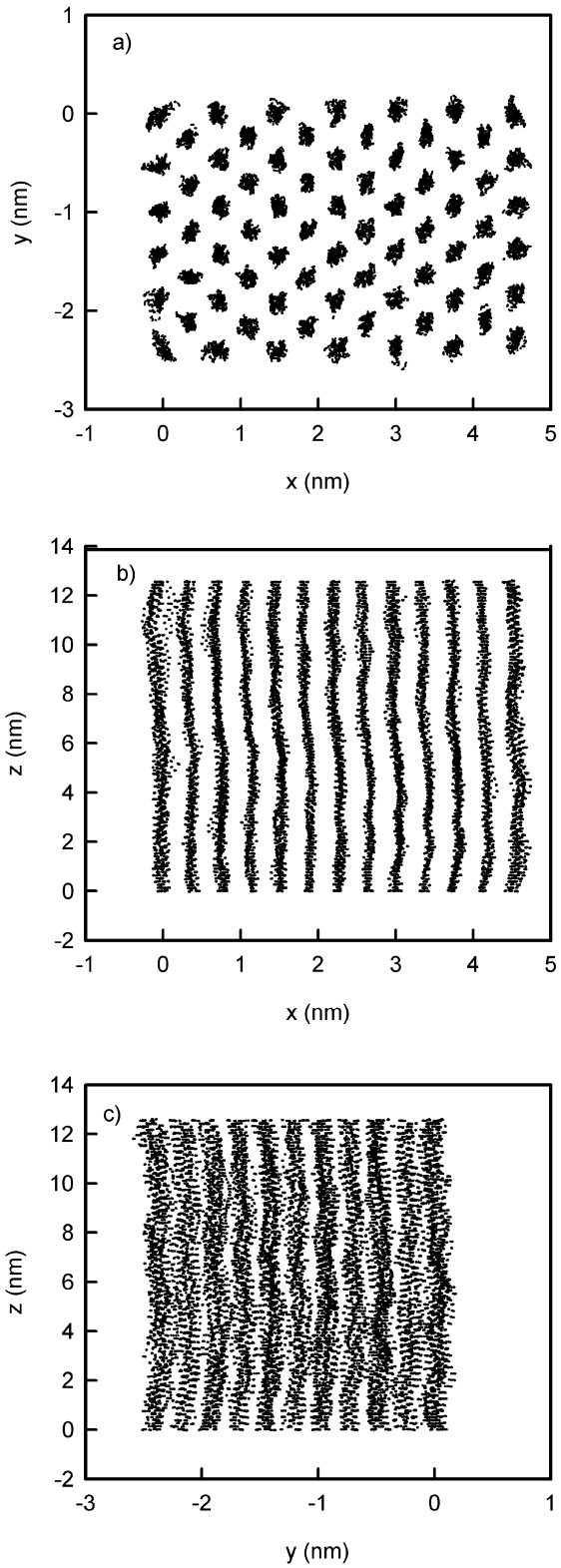

Fig. 7. Average $x-y$ (a), $x-z$ (b) and $y-z$ (c) projections of the crystal during 1.5 ps in the simulations at $T = 217$ K.

parameters may be explained by the fact that our crystal is only restrained in the z-direction. We note a slight increase with the temperature as it has already been shown in a previous study [24]. The α, β and γ parameters have been determined from the scalar product over all the vectors along $y-z$, $x-z$ and $x-y$ axes, respectively. We find $\alpha = 90.0 \pm 0.4°$, $\beta = 90.0 \pm 0.1°$ and $\gamma = 90.2 \pm 0.5°$. Such agreement between initial and mean lattice parameters has already been obtained with simulations of constrained crystals [4]. The calculations of the lattice parameters clearly show that the steady state structure from our simulations using the UA potential is the orthorhombic phase and not the hexagonal phase.

The analysis of the $(y-z)$, $(x-z)$ and $(x-y)$ projections show that the crystal maintains its solid structure during the simulation. As a consequence, the analytical form of the potential used are efficient to constrain the united sites to their equilibrium positions. The increase in temperature has no influence on the structure of the crystal. Obviously, we observe a slight increase in the binding, bending and torsional energetic contributions whereas the change in the non-bonded interactions are less marked as shown in Table 3. These characteristics suggest that the structure did not vary with the range of temperature studied here. Further insights into the local environment can be obtained with the plots of the intramolecular and intermolecular radial distribution functions.

An important property is the pair correlation function $g(r)$ which describes the local structure and can be calculated by the operational definition

$$g(r) = n(r)/4\pi^2\Delta r \tag{16}$$

where $n(r)$ is the mean number of pairs having separations between r and $r + \Delta r$, and ρ is the number of atoms divided by the volume of the simulation cell. The intra- and intermolecular radial distributions functions for CH_2-CH_2 interactions are displayed in Fig. 8. The large narrow peak in the intramolecular radial $g_{CH_2-CH_2}$ distribution function is due to the C–C covalent bonds at 1.53 Å. The successive peaks correspond to CH_2 united atoms separated by two, three, four or more bonds, respectively. This curve shows that the inner structure of the polyethylene chain is well conserved during the simulations. The intermolecular radial $g_{CH_2-CH_2}$ exhibits a first well-pronounced peak corresponding to the nearest-neighbour intermolecular structure at about 4.9 Å. This distance is in fact the value of b unit cell. The second peak occurs at 8.8 Å and reflects the atoms located at the distances $2b$ (2×4.9) and at the diagonal of a and b, i.e. 8.8 Å, a and b being the unit cells already defined. In the second peak, there is also a smaller shoulder near $r = 8.8$ Å corresponding to the distance a (7.4 Å). Is also displayed the intermolecular radial distribution for $T = 312$ K. We can check that the two distributions are very close with a decrease of the shoulder for the second peak for the higher temperature. We pinpoint that the

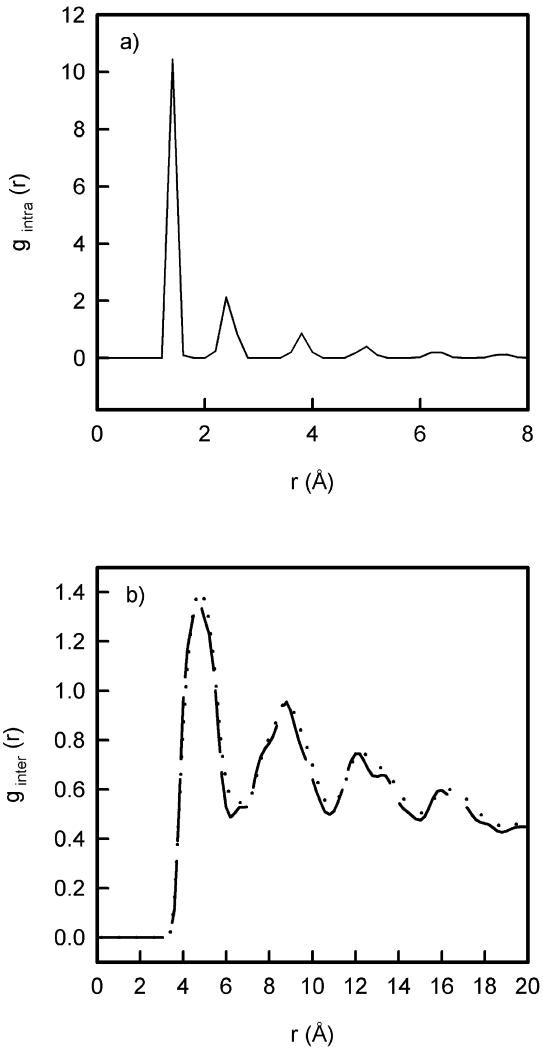

Fig. 8. (a) Intramolecular radial distribution functions $g_{CH_2-CH_2}$ and (b) intermolecular radial distribution functions $g_{CH_2-CH_2}$ at $T = 217$ K (- - -) and $T = 312$ K (···).

intermolecular distribution function do not tend to 1 due to the absence of periodic boundary conditions in the simulated system. These correlation functions confirm that the crystal is fully ordered for the two temperatures, in agreement with energetic values listed in Table 3.

4. Conclusions

We have developed a molecular dynamics algorithm in conjunction with a particular sympletic integrator capable of yielding coherent results concerning the thermodynamic parameters T and p and internal structure of the polyethylene crystal. In this paper, we have intentionally omitted the periodic boundary conditions. In doing so, we plan to study the bombardment of polyethylene by different molecules.

In a first step, we have shown that the sympletic integrator used in this study is efficient with a good conservation of the temperature and of the total energy of the system. In addition we have checked the thermal and mechanical equilibrium of our system by calculating temperature and pressure tensors. We have seen that the component presented different profiles as a function of the axes. The fact that all the on-diagonal elements of the pressure tensor are not equal may be due to unappropriated parameters in the non-bonded interaction parameters and to numerous geometric constraints. Actually, the Lennard-Jones parameters have been adjusted to reproduce thermodynamic properties in the liquid and vapour phases as enthalpies of vaporization, liquid or vapour densities. These LJ parameters have not been adjusted for the solid state. This type of problem has been already mentioned in a previous study [5]. The development of new non-bonded interaction parameters or the use of new analytical potentials for the study of solid structure is far from being completed. Anyway, the calculation of the pressure tensor different profiles along different directions represents a prerequisite before the study of bombardment of polyethylene. In addition, these simulations reveal that the two different method (IK) and (MOP) for the calculation of the pressure tensor give similar profiles in our crystal and represent two efficient algorithms for the computation of the pressure in a solid state.

The analysis of the intra- and interradial distribution functions has allowed to assign all the peaks by checking that the order inside the crystal is maintained for the two temperatures studied here.

These simulations establish our MD algorithm as a sensible tool to study the equilibrium properties of polyethylene crystal. It will be possible to perform molecular dynamics simulations of particle impacts on polyethylene crystal and to use the two algorithms of pressure computations in these studies.

References

[1] Yamamoto T. Monte Carlo simulation of the crystal structure of the rotator phase of *n*-paraffins. J Chem Phys 1985;22:3791–4.
[2] Yamamoto T. Monte Carlo simulation of the crystal structure of the rotator phase of *n*-paraffins. II. Effects of rotation and translation of the rigid molecules. J Chem Phys 1988;89:2356–65.
[3] Neyertz S, Brown D, Tomas OJ. Molecular dynamics simulation of crystalline poly(ethylene oxide). J Chem Phys 1994;101:10064–73.
[4] Liang GL, Noid DW, Sumpter BG, Wunderlich B. Structure and mass transport in constrained polymer crystals via molecular dynamics simulations. Polymer 1995;36:109–27.
[5] Brown D, Neyertz S. A general pressure tensor calculation for molecular dynamics simulations. Mol Phys 1995;84:577–95.
[6] Martonak R, Paul W, Binder K. Monte Carlo simulation of crystalline polyethylene. Comput Phys Commun 1996;99:2–8.
[7] Beardmore K, Smith R, Webb RP. Energetic fullerene interactions with Si crystal surfaces. Modelling Simul Mater Sci Engng 1994;2:313–28.
[8] Beardmore K, Smith R. Ion bombardment of polyethylene. Nucl Instrum Meth B 1995;102:223–7.

[9] Beardmore K, Smith R, Richter A, Mertesacker B. The interaction of C60 with hydrogen plasma. Vacuum 1995;46:1091–6.
[10] Brunet L, Andre P, Lombard JM, Caillau F. Thermodynamic assessment of a nitro-organic plasma with an experimental design method. IEEE Trans Magn 1999;35:185–8.
[11] Lombard JM, Bashung B, Grune D, Carriere A, Andre P. 19th Symposium of ballistics; May 2000. Interlaken 171.
[12] Andre P, Brunet L. Theoretical computation of the electrical conductivity of the thermal plasmas. Applications to plasma torch design of an electrothermal launcher. IEEE Trans Plasma Sci 2001; 29:19–28.
[13] Brenner DW. Empirical potential for hydrocarbons for use in simulating the chemical vapor deposition of diamond films. Phys Rev B 1990;42:9458–71.
[14] Brenner DW. Erratum. Empirical potential for hydrocarbons for use in simulating the chemical vapor deposition of diamond films. Phys Rev B 1992;46:1948.
[15] Sumpter BG, Noid DW, Wunderlich B. Computer experiments on the internal dynamics of crystalline polyethylene. Mechanistic details of conformational disorder. J Chem Phys 1990;93:6875–89.
[16] Hulburt HM, Hirschfelder JO. Potential energy functions for diatomic molecules. J Chem Phys 1941;9:61–9.
[17] Hulburt HM, Hirschfelder JO. Erratum. Potential energy functions for diatomic molecules. J Chem Phys 1961;35:1901.
[18] Gray SK, Noid DW, Sumpter BG. Symplectic integrators for large scale molecular dynamics simulations: a comparison of several explicit methods. J Chem Phys 1994;101:4062–72.
[19] Sanz-Serna JM. Symplectic integrators for Hamiltonian problems: an overview. Acta Numerica 1991;243–86.
[20] Walton JPRB, Tildesley DJ, Rowlinson JS. The pressure tensor at the planar surface of a liquid. Mol Phys 1983;48:1357–68.
[21] Walton JPRB, Tildesley DJ, Rowlinson JS. Erratum. The pressure tensor in an inhomogeneous fluid of non-spherical molecules. Mol Phys 1986;58:1013.
[22] Tsai DH. The virial theorem and stress calculation in molecular dynamics. J Chem Phys 1979;70:1375–82.
[23] Todd BD, Evans DJ, Daivis PJ. Pressure tensor for inhomogeneous fluids. Phys Rev E 1995;52:1627–38.
[24] Rutledge GC, Lacks DJ, Martonak R, Binder K. A comparison of quasi-harmonic lattice dynamics and Monte Carlo simulation of polymeric crystals using orthorombic polyethylene. J Chem Phys 1998;108:10274–80.